Research Article

Thu T. A. Le, Bao H. Dang, Thanh Q. C. Nguyen, Dam P. Nguyen, and Giao H. Dang*

Highly efficient removal of tetracycline and methyl violet 2B from aqueous solution using the bimetallic FeZn-ZIFs catalyst

https://doi.org/10.1515/gps-2023-0122
received July 07, 2023; accepted October 01, 2023

Abstract: Residual antibiotics and organic dyes in wastewater have gained the current challenge all over the world because of their toxicity to humans and the environment. In this study, the bimetallic porous FeZn-ZIFs materials were successfully prepared under mild conditions at room temperature and atmospheric pressure and characterized by various techniques. The FeZn-ZIFs were used as a heterogeneous catalyst to remove tetracycline antibiotics (TC) and methyl violet 2B dyes (MV) in an aqueous solution by activating peroxymonosulfate (PMS) and peroxydisulfate (PDS), respectively. The catalytic activity of FeZn-ZIFs towards TC and MV under different oxidant dosages, the catalyst dosage, the initial pollutant concentration, contact time, and reaction temperature were optimized. The results indicated that FeZn-ZIFs was an efficient catalyst for removing TC and MV based on advanced oxidant processes, having a removal capacity of 92% at TC concentration of 50 $mg{\cdot}L^{-1}$ and 95% MV concentration of 20 $mg{\cdot}L^{-1}$. More importantly, this bimetallic catalyst was identified the superior structural stability when the removal efficiency of TC and MV was maintained at approximately 90% after five cycles. In short, the FeZn-ZIFs and PMS/PDS system exhibited a promising application prospect for antibiotic and dye-containing wastewater treatment.

Keywords: advanced oxidation process, bimetallic, methyl violet 2B, tetracycline, zeolitic imidazolate framework

*** Corresponding author: Giao H. Dang,** College of Engineering, Can Tho University, Campus II, 3/2 Street, Ninh Kieu District, Can Tho City, Vietnam; Applied Chemical Engineering Lab, College of Engineering, Can Tho University, Campus II, 3/2 Street, Ninh Kieu District, Can Tho City, Vietnam, e-mail: dhgiao@ctu.edu.vn, tel: (+84) 292 3834267; fax: (+84) 292 383115
Thu T. A. Le, Bao H. Dang: College of Engineering, Can Tho University, Campus II, 3/2 Street, Ninh Kieu District, Can Tho City, Vietnam
Thanh Q. C. Nguyen: College of Natural Science, Can Tho University, Campus II, 3/2 Street, Ninh Kieu District, Can Tho City, Vietnam
Dam P. Nguyen: Department of Chemistry Education, Can Tho University, Campus II, 3/2 Street, Ninh Kieu District, Can Tho City, Vietnam

1 Introduction

Environmental contamination, especially water pollution, has been a global concern that needs to be addressed due to its severe impact on organisms and ecosystems [1]. Along with the growth of population, industrialization, and modernization, the amount of wastewater increased drastically, often containing organic dyes, antibiotic residues, heavy metals, pesticides, and industrial chemicals...[2]. This wastewater poses a threat to the environment and quality of human life [3]. For instance, the antibiotic residues found in wastewater can form antibiotic resistance genes that make the infections caused by resisted bacteria have become complicated and costly for treatment [4,5]. Meanwhile, the presence of dyes in the aqueous environment is proven to be toxic and relates to several dreadful human diseases, including skin irritation, kidney failure, intestinal tract infection, and even carcinogenicity [6]. Typically, tetracycline antibiotic (TC) and methyl violet 2B dye (MV) are the organic compounds which have been commonly used to fulfill human needs. TC is the world's second most widely used antibacterial chemical and one of the primary antibiotics used in the treatment of human diseases, aquaculture, and livestock production [7]. However, the hydrophilic and hard to metabolize completely by human or animal organisms nature of TC leads to its considerable persistence in water bodies [8]. On the other hand, MV is a cationic triphenylmethane dye widely used in textile industries, paper printing, ink making, and other fields [9,10]. This dye gives an intensive violet color when dissolved in water, even with small concentrations [11]. Because of their complex and durable chemical structure with many aromatic rings, they usually accumulate in aquatic environments. Remarkably, these contaminants are not only toxic but also stable to heat, light, and hardly

Open Access. © 2023 the author(s), published by De Gruyter. This work is licensed under the Creative Commons Attribution 4.0 International License.

biologically degradable [12–14]. Therefore, a variety of methods for removing antibiotics and dye from aquatic environments have been extensively investigated, including adsorption, coagulation, flocculation, membrane filtration, photocatalytic degradation, and biological treatment [15–18]. Among these methods, advanced oxidation processes (AOPs) have attracted the attention of scientists due to their mineralization ability to organic contaminants present in wastewater [19,20]. Namely, AOPs involve the generation of highly reactive radical species, which are powerful oxidizing agents and capable of attacking a wide variety of organic molecules to nontoxic and simple molecules based on the oxidants including hydrogen peroxide (H_2O_2), peroxymonosulfate (PMS) (HSO_5^-), peroxydisulfate (PDS) ($S_2O_8^{2-}$), ozone (O_3), and permanganate (MnO_4^-) [21]. There are many ways to activate the oxidant agent in the AOPs, such as thermal excitation, ultraviolet radiation, and other methods that require additional energy [22]. Recently, the heterogeneous catalytic system consisting of transition metals (Co, Zn, Mn, and Fe) and PMS/PDS has been shown to degrade antibiotics and dye efficiently [23]. However, because of interactions with strong oxidizing agents, the catalyst material needs to ensure durability and certain requirements such as porous nature, a large specific surface, high stability, and diverse structure and composition to bring high efficiency [24]. Therefore, designing heterogeneous catalysts with outstanding properties to activate the oxidant effectively is challenging for scientists.

Accordingly, zeolitic imidazolate frameworks (ZIFs) are the potential candidates for the AOPs because of their inherent superior properties such as large pore volume, tunable porosity, ultrahigh specific surface area, high thermal stability, and molecular and structural diversity [25,26]. Namely, ZIFs is a subclass of metal-organic framework material that is structurally similar to zeolite, but its composition is a combination of both inorganic ions and organic bridges [27]. Typically, ZIFs are formed from the metallic nodes (i.e., Zn and Co) and linked together by imidazolate organic bridges through self-assembly arrangement. ZIFs have become attractive to scientists in many fields, such as adsorption, catalysis, gas storage, chemical separation, and drug delivery [28,29]. Some researchers have reported that ZIFs are highly effective for removing antibiotics and dyes. Indeed, Li et al. prepared ZIF-8 for the adsorption of TC and oxytetracycline (OTC) which the maximum adsorption capacities for TC and OTC were 303 and 312.5 $mg \cdot g^{-1}$, respectively [30]. The proposed adsorption mechanism likely involved π–π interactions between the conjugated groups in TC/OTC and the imidazole rings of ZIF-8. In addition, the presence of metal in ZIFs also contributes to promoting the catalytic potential of the material for the decomposition process and eliminating the toxicity of the pollutant. In 2021, Tran and Nguyen reported a facile method to synthesize ZIF-67 under a one-step hydrothermal reaction from cobalt salt in methanol with high photostability and easy reusability [31]. In a neutral medium, more than 88% of methyl orange (MO) was degraded within 1 h with the presence of as-prepared ZIF-67. Recently, many research articles have suggested that combining two metal centers in a ZIF structure can improve many outstanding properties of the material and bring high catalytic ability. Namely, Abuzalat et al. successfully synthesized the bimetallic Co/Zn-ZIF-8 as an efficient catalyst to promote H_2O_2 oxidation to remove MO dye [32]. The Co/Zn-ZIF-8/H_2O_2 system successfully decolorized more than 90% MO (10 $mg \cdot L^{-1}$) at pH 6.5 within only about 50 min.

In this study, a green and straightforward strategy is proposed to synthesize the bimetallic FeZn-ZIFs as a heterogeneous catalyst for removing pollutants based on AOPs. The properties of Fe-doped ZIF-8 are also investigated and characterized. Herein, TC antibiotic and methyl violet 2B dye are used as a pollutant model. The removal behavior of FeZn-ZIFs is examined in detail, including catalyst dosage, oxidant dosage, different concentrations of TC and MV, contact time, and reaction temperature. Furthermore, the stability of the catalyst is also determined through the efficiency of reusability and structural characterization reanalysis using Powder X-ray diffraction (PXRD) and Fourier transform infrared spectroscopy (FT-IR) methods.

2 Materials and methods

2.1 Materials

2-Methylimidazole (2-MIm, $C_4H_6N_2$, 99%) was purchased from Acros. Zinc nitrate hexahydrate ($Zn(NO_3)_2 \cdot 6H_2O$, 99%), iron (II) sulfate heptahydrate ($FeSO_4 \cdot 7H_2O$, 99%), potassium peroxydisulfate (PDS, $K_2S_2O_8$, 99.5%), MV 2B ($C_{24}H_{28}ClN_3$, 80% dye content) and methanol (MeOH, CH_3OH, 99.5%) were purchased from Xilong Chemical Co., Ltd, China. Potassium PMS, ($KHSO_5 \cdot 0.5KHSO_4 \cdot 0.5K_2SO_4$, containing 47% $KHSO_5$) was purchased from Sigma Aldrich. TC hydrochloride ($C_{22}H_{24}N_2O_8 \cdot HCl$) was purchased from Bomei, China, with a high purity grade. All the reagents were used as received without further purification.

2.2 Synthesis of FeZn-ZIFs

FeZn-ZIFs were synthesized by the solvothermal method, as reported in a previous study with slight modifications [33].

For the synthesis of the FeZn-ZIFs, 4.5 mmol of $Zn(NO_3)_2{\cdot}6H_2O$ and 0.5 mmol of $FeSO_4{\cdot}7H_2O$ were completely dissolved in 25 mL MeOH. Next, this homogenized mixture was added dropwise into 25 mL MeOH solution containing 20 mmol of 2-MIm under magnetic stirring. A light yellow suspension was gradually formed, which was then aged 24 h at room temperature. Subsequently, the crystals were collected by centrifugation at 4,000 rpm within 10 min, purified in MeOH several times, dried overnight at 60°C, and obtained light–yellow FeZn-ZIFs powder.

Besides, some other heterogeneous catalysts, including ZIF-8, ZnCo-ZIFs, CuZn-ZIFs, and FeCo-ZIFs, were also synthesized based on the reported procedures with slight modifications for comparison. Herein, ZIF-8 crystals were prepared by solvothermal reaction of $Zn(NO_3)_2{\cdot}6H_2O$ (1.485 g, 5 mmol) and 2-MIm (1.64 g, 20 mmol) in 40 mL MeOH [34]. Similarly, ZnCo-ZIFs were also synthesized by the solvothermal method of $Co(NO_3)_2{\cdot}6H_2O$ (0.873 g, 3 mmol), $Zn(NO_3)_2{\cdot}6H_2O$ (0.297 g, 1 mmol) and 2-MIm (1.3136 g, 16 mmol) in 30 mL MeOH [35]. For the synthesis of the CuZn-ZIFs, crystals were obtained by reaction of $Zn(NO_3)_2{\cdot}6H_2O$ (0.891 g, 3 mmol), $Cu(NO_3)_2{\cdot}3H_2O$ (0.242 g, 1 mmol) and 2-MIm (1.3136 g, 16 mmol) in 40 mL MeOH [36]. Finally, FeCo-ZIFs were synthesized by $Co(NO_3)_2{\cdot}6H_2O$ (0.7275 g, 2.5 mmol), $FeSO_4{\cdot}7H_2O$ (0.139 g, 0.5 mmol), and 2-MIm (3.9408 g, 48 mmol) in 40 mL MeOH [37].

2.3 Characterization of FeZn-ZIFs

PXRD patterns of FeZn-ZIFs particles were collected on an Empyrean-PANanlytical powder diffractometer with a scan range of 2θ recorded from 5 to 80 degrees. FT-IR was attained using PerkinElmer MIR/NIR Frontier instrument and recorded from 400 to 4,000 cm^{-1}. Thermogravimetric analysis (TGA) of the powder was conducted in the N_2 gas from a temperature of 800°C with a heating rate of 10°C·min^{-1} using LabSys Evo TG-DSC 1600 instrument. Surface morphology and particle size were observed by scanning electron microscopy (SEM, Hitachi S-4800). Energy dispersive X-ray (EDX) was used to analyze the elemental components present in the material. The specific surface areas of the samples were calculated using Brunauer–Emmett–Teller (BET) method.

2.4 Catalyst experiments

TC antibiotic and MV 2B dye were used as a pollutant model to evaluate the catalytic activity of the FeZn-ZIFs material in the presence of potassium PMS and potassium PDS, respectively. Typically, a certain amount of the as-prepared catalyst sample (0–0.5 g·L^{-1}) was dispersed into 10 mL of pollutant solution in a different concentration (5–70 mg·L^{-1}) with the presence of the oxidant dosage (0–0.5 g·L^{-1}). The mixture was performed under magnetic stirring at various time intervals (15–75 min) and temperatures (from room temperature to 70°C). After the reaction, the catalyst and solution were separated by filtration and centrifugation. A UV–visible spectrophotometer was used to analyze the residual concentrations of TC and MV at wavelengths 357 and 583 nm, respectively. The removal efficiency was computed by the following equation:

$$\text{Removal efficiency (\%)} = \frac{C_0 - C_t}{C_0} \times 100 \quad (1)$$

where C_0 and C_t are the initial TC and MV concentration (mg·L^{-1}) and the pollutant concentration at time t, respectively (mg·L^{-1}).

A 100 mg·L^{-1} stock solution of pollutants was prepared by dissolving 0.01 g of the pollutants in 100 mL of distilled water. The other pollutant concentrations used in the experiment were done by diluting the stock solution with suitable volumes of distilled water. In particular, because hydrolysis and precipitation of TC in water can occur, the TC stock solution was renewed just before each use.

2.5 Reusability of FeZn-ZIFs

The reusability of FeZn-ZIF catalyst was carried out under the optimal condition of the TC and MV removal. After each iteration, the catalyst was separated by centrifugation, washed several times with MeOH, and dried overnight at 60°C to recover for the next cycle. Upon completion, the recovered catalyst was re-tested to demonstrate its structural stability by PXRD and FT-IR methods.

3 Results and discussion

3.1 Characterization of FeZn-ZIFs catalyst

The FeZn-ZIFs catalyst was synthesized by solvothermal method at room temperature and MeOH solvent according to a previously reported procedure by Yang et al. with slightly modified [33]. The PXRD analysis was analyzed to examine the crystal structure of FeZn-ZIFs compared with ZIF-8, as presented in Figure 1(a).

The result showed that FeZn-ZIFs exhibited a similar PXRD spectrum as the pristine ZIF-8 with the prominent peaks indexed to (011), (002), (112), (022), (013), (222), (114), (233), (134), and (334) corresponding to 2θ values of 7.3°,

10.3°, 12.7°, 14.9°, 16.3°, 22.1°, 24.9°, 25.5°, and 26.5°, respectively. Notably, a characteristic peak with an obvious signal existed at 2θ of 7.3° in both PXRD patterns of FeZn-ZIFs and ZIF-8, indicating that they were highly crystalline, which was in excellent agreement with a previous report [38]. Thus, the comparison of PXRD results demonstrated the isomorphic substitution of Fe^{2+} and Zn^{2+}, which could be due to the similar ionic size between these two elements [39]. In other words, Fe^{2+} partially replaced Zn^{2+} and formed the bimetallic framework FeZn-ZIFs without breaking the original structure of ZIF-8.

The FT-IR spectra were recorded to confirm the presence of functional groups and chemical bonds in the FeZn-ZIFs. The results are shown in Figure 1(b). The bands appearing in the range of 600–1,500 cm^{-1} could be attributed to imidazole stretching and bending modes which were supposed to be the bridge of metal nodes presented in both 2-MIm and FeZn-ZIFs. Notably, the presence of the major absorbance peak at 1,846.1 cm^{-1} indicated the N-H stretching vibration in FT-IR of 2-MIm, whereas it completely disappeared in FT-IR of FeZn-ZIFs, demonstrating that de-protonation of N-H group of 2-MIm. Instead, a new absorption band at 421.6 cm^{-1} was assigned to the Fe–N or Zn–N stretching, consistent with the previous report of Zhou and co-workers [40]. More than that, the EDX measurement verified the presence of the elements, including C, N, especially Fe, and Zn, which validated the incorporation of both Fe and Zn within the same framework (Figure 1(d)).

The morphology and particle size were observed through scanning electron microscopy (Figure 1(e)). The result exhibited the rhombic dodecahedron structure of FeZn-ZIFs. The particle size distribution was uneven in the ratio and fluctuated from 100 nm to 5 µm. Accordingly, the initial metal salt source, stirring speed, a ratio of metal salt and 2-MIm, as well as the temperature of the reaction system are the factors affecting the surface morphology and the size of the crystals [41]. Additionally, the BET analysis of FeZn-ZIFs showed that the specific surface area was at 1,171.7 $m^2 \cdot g^{-1}$ (Figure S5). The thermal stability of FeZn-ZIFs was studied by TGA, as displayed in Figure 1(c). The result showed that the weight was slightly undermined when increasing the temperature to 100°C, and a sharp decline occurred between 350°C and 700°C, which is caused by the framework collapse of the material in the high temperature. Based on the previous discussion, the combination of Fe and Zn in the same structural framework not only preserves the inherent thermal stability of ZIFs but also creates a new material with a more diverse composition, providing multiple catalytic sites that promise to bring new materials with more potential applications.

3.2 Catalyst activity of FeZn-ZIFs on TC and MV treatment

The catalytic potential of FeZn-ZIFs was investigated using the removal of TC and MV based on AOPs. An oxidizing agent is one of the important factors in this process. Therefore, the dosage of oxidant was investigated and observed in Figure 2. The result indicated that enhancing

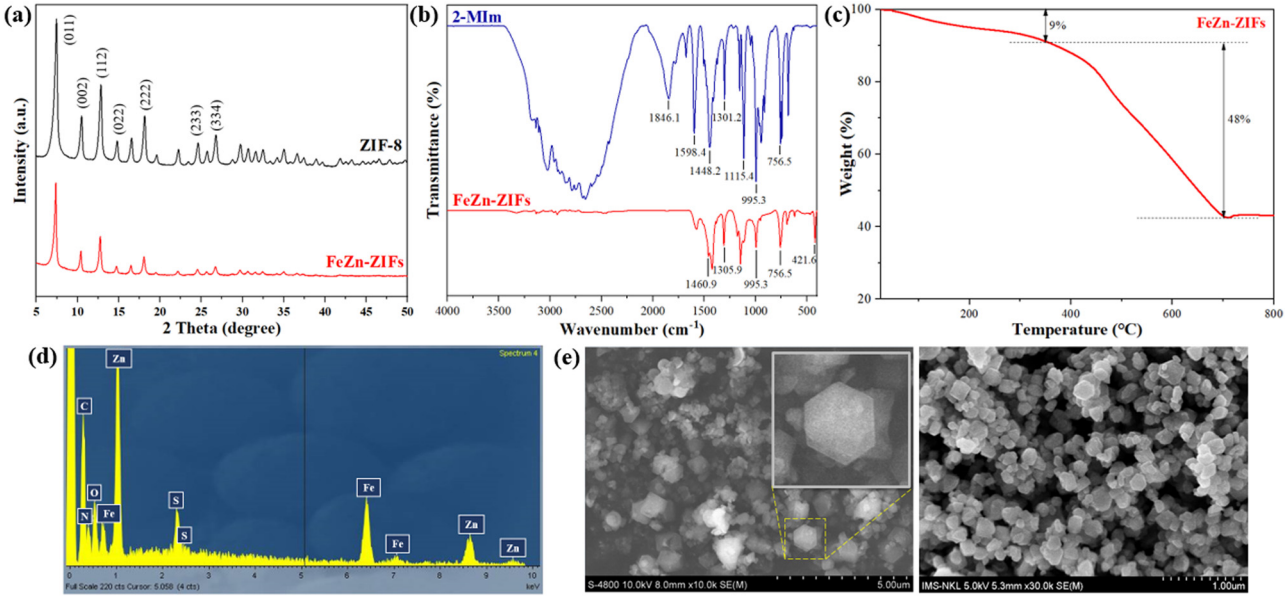

Figure 1: (a) PXRD patterns of ZIF-8 and FeZn-ZIFs, (b) FT-IR patterns of 2-MIm and FeZn-ZIFs, (c) TGA curve of FeZn-ZIFs, (d) EDX spectrum of FeZn-ZIFs, and (e) SEM images of FeZn-ZIFs.

oxidant dosage caused an increment in the efficiency of the TC and MV removal. In the absence of oxidant, the efficiency removal of the TC (the initial concentration of 50 mg·L^{-1}) and MV (the initial concentration of 20 mg·L^{-1}) was 57% and 27%, respectively. This may be the adsorption capacity of FeZn-ZIFs due to the porous nature and the large specific surface area (1,171.7 m^2·g^{-1}). However, the main purpose of this study is pollutant degradation through the AOPs, so PMS and PDS were added to the process removal of TC and MV, respectively, to create the sulfate radicals ($SO_4^{\cdot-}$) under the catalysis of FeZn-ZIFs according to Eqs. 2–5 [42,43]:

$$Fe^{2+} + HSO_5^- \rightarrow Fe^{3+} + SO_4^{\cdot-} + OH^- \quad (2)$$

$$Fe^{2+} + S_2O_8^{2-} \rightarrow Fe^{3+} + SO_4^{\cdot-} + SO_4^{2-} \quad (3)$$

$$SO_4^{\bullet-} + H_2O \rightarrow SO_4^{2-} + {}^{\cdot}OH + H^+ \quad (4)$$

$$SO_4^{\cdot-} + {}^{\cdot}OH + MV \rightarrow \text{By-products} + CO_2 + H_2O + SO_4^{2-} \quad (5)$$

Besides, some reports suggested that adding a large amount of PMS or PDS can generate more free radicals and boost the pollutant removal efficiency in the heterogeneous reaction but excessive PMS or PDS can quench free radicals and be detrimental to the process [44,45]. Moreover, sulfate is a free radical with a strong oxidizing ability, so it can affect the durability of the catalyst structure if used excessively. So, the use of large amounts of oxidant is not necessary. Hence, the following catalytic experiments were carried out under the oxidant dosage at 0.4 g·L^{-1} for TC and 0.3 g·L^{-1} for MV.

The bimetallic FeZn-ZIFs play a catalytic role in activating the oxidant (PMS or PDS) to generate sulfate radicals. Therefore, the FeZn-ZIFs dosage was investigated to consider its effect on removing TC and MV (Figure 3). As shown in Figure 3, the catalytic performance was obviously improved by increasing the catalyst concentration from 0 to 0.5 g·L^{-1}. Namely, TC removal efficiency increased from 70% to 92% when the catalyst dosage increased from 0 to 0.5 g·L^{-1} while the removal capacity for MV increased from 76% to 96%, respectively. Actually, a higher catalyst concentration can provide more active sites, which is conducive to the activation of oxidants and promotes the degradation efficiency of pollutants. However, the result showed that the TC removal efficiency at the catalyst dosages of 0.4 and 0.5 g·L^{-1} was maintained at 92%. For MV, when the catalyst concentration increased from 0.3 to 0.5 g·L^{-1}, the removal efficiency of TC was improved slightly. This increase in pollutant removal efficiency may be due to active-species production. Although a large number of catalysts can provide more active sites to activate the oxidant, an excessive amount of FeZn-ZIFs stalls the reaction due to its rapid reaction with $SO_4^{\cdot-}$ and $S_2O_8^{2-}$ [46], the scavenging effect of oxidants toward radicals [47], and the self-combination reactions of radicals [48], resulting in lower efficiency of contaminant removal in systems ((Eqs. 6 and 7).

$$SO_4^{\cdot-} + Fe^{2+} \rightarrow Fe^{3+} + SO_4^{2-} \quad (6)$$

$$S_2O_8^{\cdot2-} + 2Fe^{2+} \rightarrow 2SO_4^{2-} + 2Fe^{3+} \quad (7)$$

Therefore, the optimal dosage of FeZn-ZIFs catalyst was determined at 0.4 and 0.3 g·L^{-1} for TC and MV removal, respectively.

Different concentrations of TC and MV were analyzed to determine the impact of the initial concentration of pollutants on removal capacity. The reaction results are displayed in Figure 4.

The survey of TC removal reaction was performed with a range of initial concentrations from 10 to 70 mg·L^{-1}. The TC removal effect decreased as the initial concentration of TC

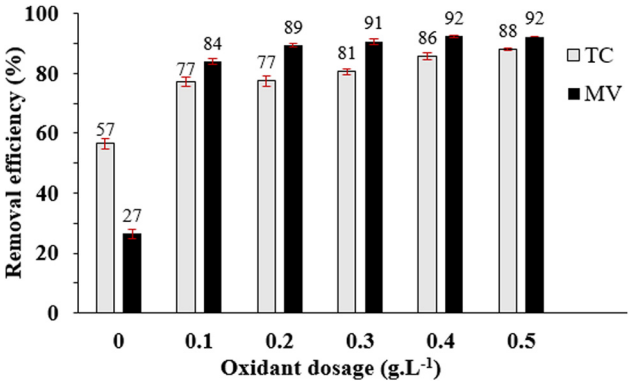

Figure 2: Effect of oxidant dosage on TC and MV removal efficiency. TC: catalyst dosage = 0.1 g·L^{-1}, [TC] = 50 mg·L^{-1}, time = 30 min, and room temperature. MV: catalyst dosage = 0.1 g·L^{-1}, [MV] = 20 mg·L^{-1}, time = 30 min, and room temperature.

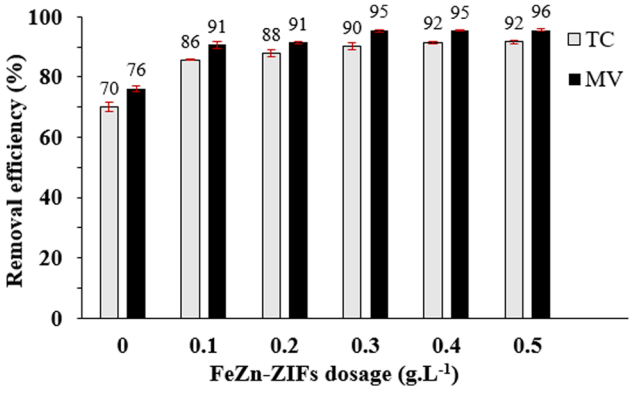

Figure 3: Effect of FeZn-ZIFs dosage on TC and MV removal efficiency. TC: PMS dosage = 0.4 g·L^{-1}, [TC] = 50 mg·L^{-1}, time = 30 min, and room temperature. MV: PDS dosage = 0.3 g·L^{-1}, [MV] = 20 mg·L^{-1}, time = 30 min, and room temperature.

increased. Obviously, the TC removal efficiency by the FeZn-ZIFs/PMS reaction system is high. The proof was this system removed 97% of 10 mg·L^{-1} TC and 86% at a high TC concentration of 70 mg·L^{-1}. The removal ability of antibiotics is due to the interaction between them and the free radicals formed at the active sites on the catalyst surface in the AOPs. When the TC concentration is high, there is competitive adsorption between oxidants and pollutants on the catalyst surface and the increase of the pollutant molecule around the active sites results in inhibiting the penetration of oxidants to the surface of the catalyst [49]. Thereby, the number of available active sites is reduced and affects the overall process efficiency. The removal efficiency for the various TC concentrations at 10, 20, 30, 40, 50, 60, and 70 mg·L^{-1} were gained 97%, 96%, 94%, 93%, 92%, 88%, and 86%, respectively. This study chose the TC concentration at 50 mg·L^{-1} as the optimal concentration.

Besides, the effect of initial MV concentration on the it removal efficiency was examined with different levels from 5 to 30 mg·L^{-1}. Figure 4 represents that removal efficiency increased when the initial MV concentration increased from 5 to 20 mg·L^{-1}, corresponding from 86% to 95%, respectively. This can be explained by the fact that at the low concentration, the collision frequency between the active sites on the surface of the catalyst and dye molecules is decreased and causes a reduction in the MV removal efficiency [50]. However, when the concentration continued to increase to 25 and 30 mg·L^{-1}, the removal efficiency decreased at 91% and 92%, respectively. This may be due to the fixation time in the reaction of 30 min, which is not enough for the FeZn-ZIFs/PDS system to remove MV at higher concentrations. Thereby, the initial concentration of MV was chosen 20 mg·L^{-1} to conduct the next experiments.

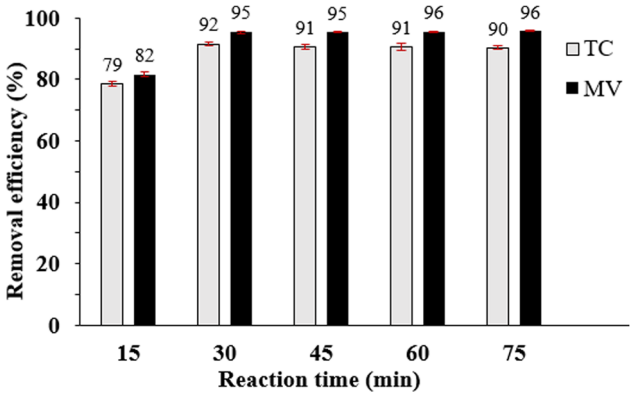

Figure 5: Effect of reaction time on TC and MV removal efficiency. TC: PMS dosage = 0.4 g·L^{-1}, catalyst dosage = 0.4 g·L^{-1}, [TC] = 50 mg·L^{-1}, and room temperature. MV: PDS dosage = 0.3 g·L^{-1}, catalyst dosage = 0.3 g·L^{-1}, [MV] = 20 mg·L^{-1}, and room temperature.

Reaction time is one of the important parameters regarding the reaction rate. Besides, the longer the reaction time, the higher the cost. Therefore, it is necessary to optimize the time at a reasonable level to both achieve pollutant removal efficiency and boost the economic efficiency of the entire process. In this study, the effect of reaction time was performed by conducting experiments at different time intervals from 15 to 75 min (Figure 5). The result showed that the longer the reaction time, the higher the pollutant removal efficiency. Specifically, the TC and MV removal efficiency of FeZn-ZIFs in the presence of oxidant was quite fast, with values of 79% and 82%, respectively, after only 15 min. When the time increased to 30 min, the performance increased to 92% for TC and 95% for MV. This can be explained that the longer the time, the higher the ability of FeZn-ZIFs to activate PMS/

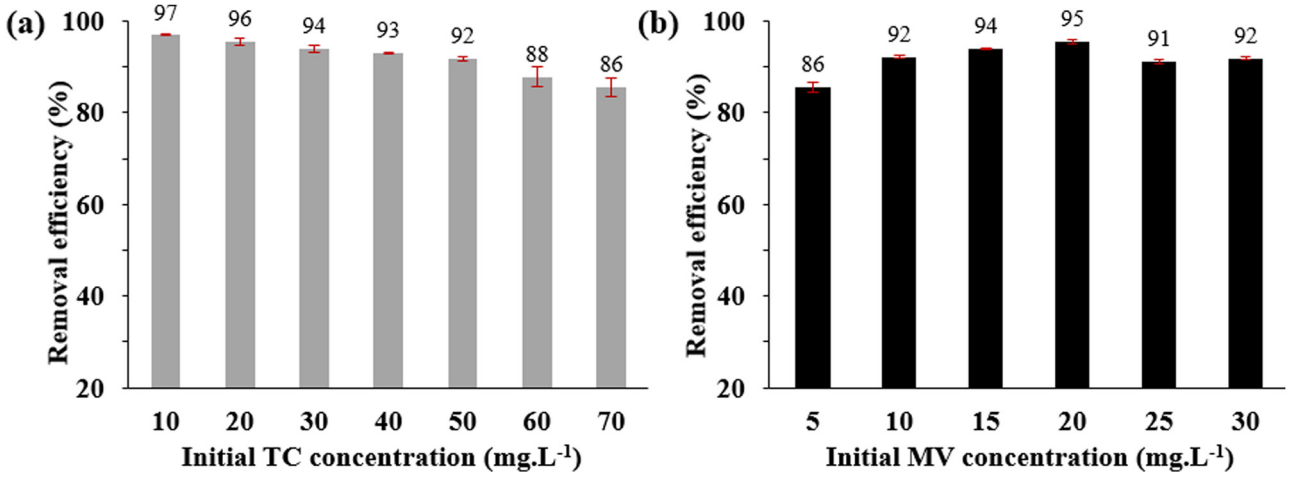

Figure 4: Effect of initial concentration of (a) TC and (b) MV on the removal efficiency. TC: PMS dosage = 0.4 g·L^{-1}, catalyst dosage = 0.4 g·L^{-1}, time = 30 min, and room temperature, (b) MV: PDS dosage = 0.3 g·L^{-1}, catalyst dosage = 0.3 g·L^{-1}, time = 30 min, and room temperature.

PDS to produce sulfate radicals and create conditions for the pollutant to decompose more. However, at time levels after 30 min, the removal efficiency of both TC and MV tended to remain in equilibrium, with values ranging from 90% to 91% for TC and 95–96% for MV. Therefore, 30 min was an appropriate time for both TC and MV removal processes.

Temperature is also one of the essential parameters for pollutant removal studies because it is directly related to the kinetics and reaction rate. The TC and MV removal experiments were performed at room temperature, 50°C, 60°C, and 70°C, respectively, as shown in Figure 6. It is clearly indicated that the removal capacity of TC and MV was influenced by the temperature, even though the augment was not obvious. The performance was only 1% to 2% difference at the survey levels. Namely, the TC removal efficiency ranged from 90% to 92% and 95% to 96% for MV when the temperature was increased from room temperature to 70°C. Higher temperatures increased the reaction rate between the oxidizing agent and the catalyst, thus increasing the rate of generation of oxidizing species to boost the pollutant removal efficiency [50]. However, this is only true for the MV removal reaction system. Typically, at room temperature and 50°C, the removal efficiency reached 95% and increased slightly to 96% when the temperature was at 60°C and 70°C. For TC, the removal efficiency tended to slightly decrease with increasing temperature, but it did not change significantly. In terms of economy, a lower temperature might reduce the process cost, so the room temperature was chosen as the most suitable temperature for this process.

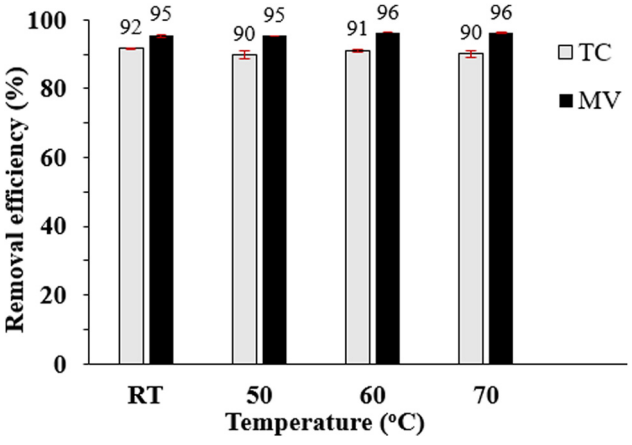

Figure 6: Effect of reaction temperature on TC and MV removal efficiency. TC: PMS dosage = 0.4 g·L^{-1}, catalyst dosage = 0.4 g·L^{-1}, [TC] = 50 mg·L^{-1}, and time = 30 min. MV: PDS dosage = 0.3 g·L^{-1}, catalyst dosage = 0.3 g·L^{-1}, [MV] = 20 mg·L^{-1}, and time = 30 min.

3.3 The efficiency of TC and MV removal using FeZn-ZIFs in comparison with other catalysts

In addition to the above investigations, the bimetallic FeZn-ZIFs are also used to compare the catalytic activity with other heterogeneous catalysts, including ZIF-8, ZnCo-ZIFs, CuZn-ZIFs, and FeCo-ZIFs under the same conditions for each pollutant. The optimum conditions for TC and MV removal included oxidant dosage, catalyst dosage, initial pollutant concentration, reaction time, and reaction temperature from previous experiments were used. For TC, they were 0.4 g·L^{-1} PMS, 0.4 g·L^{-1} catalyst, 50 mg·L^{-1} TC, 30 min, and room temperature, respectively. The optimal conditions of MV removal were 0.3 g·L^{-1} PDS, 0.3 g·L^{-1} catalyst, 20 mg·L^{-1} MV, 30 min, and room temperature, respectively. The experiments were conducted and recorded based on the removal efficiency of TC and MV as presented in Table 1.

In this experiment, the catalytic efficiency of FeZn-ZIFs was highest in both TC and MV removal processes. The result indicated that when using pristine ZIF-8, the removal efficiency of TC was not as good as that of the bimetallic FeZn-ZIFs. Namely, ZIF-8 removed 74% TC; meanwhile, FeZn-ZIFs reached 92% in the same conditions. Similarly, the MV removal efficiency of ZIF-8 was 5% lower than that of FeZn-ZIFs. This showed that metal doping in the structural framework of ZIFs has contributed to an increase the catalytic activity of ZIFs. Besides, some heterogeneous catalysts also showed the removal capability of TC and MV, possibly depending on the nature of the ZIFs and the activity of the active sites contained in that material in the following mechanism [23,51]:

Table 1: Comparison of TC and MV removal efficiency among heterogeneous catalysts and FeZn-ZIFs

The heterogeneous catalysts	FeZn-ZIFs	ZIF-8	ZnCo-ZIFs	CuZn-ZIFs	FeCo-ZIFs
The removal efficiency of TC (%)	92	74	78	87	89
The removal efficiency of MV (%)	95	90	87	90	88

$$S_2O_8^{2-} + M^n \rightarrow M^{n+1} + SO_4^{\cdot-} + SO_4^{2-} \quad (8)$$

$$HSO_5^- + M^n \rightarrow M^{n+1} + SO_4^{\cdot-} + OH^- \quad (9)$$

where M is transition metal (such as Fe^0, Fe^{2+}, Cu^{2+}, Co^{2+}, Zn^{2+}...) and n is the corresponding valence.

In addition, the related studies on the methods to degrade organic pollutants by different materials in recent years were summarized in Table 2. Despite the difficulty in comparing FeZn-ZIFs with other reported materials due to diverse experimental conditions and methods. However, compared with the previous literatures presented in the summary table, the as-synthesized FeZn-ZIFs in this study have better catalytic performance for TC and MV removal.

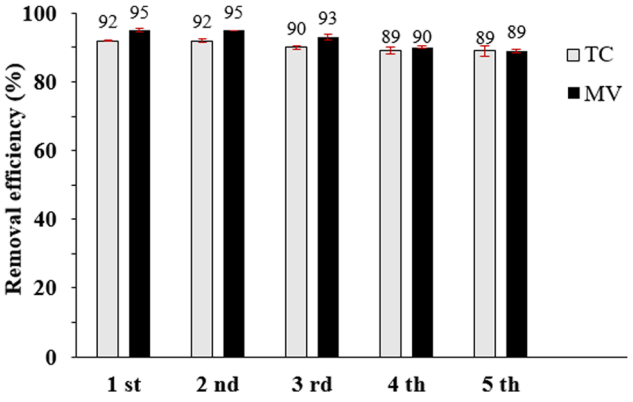

Figure 7: Efficiency of FeZn-ZIFs reusability after TC and MV treatment under optimal conditions. TC: PMS dosage = 0.4 g·L^{-1}, catalyst dosage = 0.4 g·L^{-1}, [TC] = 50 mg·L^{-1}, time = 30 min, and room temperature. MV: PDS dosage = 0.3 g·L^{-1}, catalyst dosage = 0.3 g·L^{-1}, [MV] = 20 mg·L^{-1}, time = 30 min, and room temperature.

3.4 The efficiency of FeZn-ZIFs reusability after TC and MV treatment

The recovery of catalysts is one of the important standards of heterogeneous catalysis [64]. The utilization of heterogeneous catalysts in the reaction system is an economically and cost-effective solution due to its reusability capacity. Therefore, the bimetallic FeZn-ZIFs catalyst evaluated the stability and reusability after using TC and MV treatment at optimal conditions. The results are shown in Figure 7.

Obviously, FeZn-ZIFs still had good TC and MV removal efficiency after several reusability. Namely, the removal efficiency of TC and MV decreased from 92% to 89% and 95% to 89%, respectively, after five cycles. In addition, the FeZn-ZIFs catalyst, after conducting the final cycle, was analyzed PXRD and FT-IR to confirm the structural stability. The results represented in Figure 7 showed that the peaks at the characteristic positions were maintained in the FT-IR of the recovered FeZn-ZIFs sample compared to the fresh one (Figure 8). Remarkably, the oscillation of the imidazole ring as well as the peaks at the featured positions were still guaranteed for the recovered FeZn-ZIF samples after TC and MV treatment, although there was a little change. In comparison with the fresh FeZn-ZIFs, the infrared spectrum of the reused one had a vibration stretched at 3,430.1 cm^{-1} (reused with TC) and 3,435.4 cm^{-1} (reused with MV) which was assigned to the stretching vibration of non-hydrogen bonded H_2O and hydroxyl (−OH) groups [65,66]. Furthermore, the featured peaks of the metal-N binding sites are still signaled with a slight displacement from 421.6 to 422.7 cm^{-1} (for reused with TC) and 423.7 cm^{-1} (reused with MV). These discussions indicated

Table 2: Comparison of some reported materials and methods for removal capacities for TC and MV in recent years

Catalyst	Process	*C* (mg·L^{-1})	Catalyst dosage (g·L^{-1})	Time (min)	Removal efficiency (%)	Ref
AgO/MgO/FeO@Si_3N_4	Adsorption	[TC] = 30	0.6	90	80	[52]
Cu_2O/ZIF-8	Visible-light photocatalytic	[TC] = 50	0.4	120	73.5	[53]
HNTs@g-C_3N_4/Au/CdS	UV photocatalytic	[TC] = 20	0.5	120	87.4	[54]
Fe_2Co_1/NPC	Electro-Fenton	[TC] = 20	0.3	60	91	[55]
Fe-LBH	PDS-AOPs	[TC] = 20	1	30	85	[56]
CoP@Co_2P	PMS-AOPs	[TC] = 20	0.05	60	84.7	[57]
ZnS	Adsorption	[MV] = 25	0.08	120	91.4	[58]
$BiFeO_3$@TiO_2	Visible light photocatalytic	[MV] = 15	1	120	93	[59]
TiO_2/Pt	UV photocatalytic	[MV] = 10	2	20	78	[60]
Co_3O_4 NPs	UV photocatalytic	[MV] = 10	1	45	92	[61]
$CuAl_2O_4$	Sunlight photocatalytic	[MV] = 10	1	3 h	89	[62]
Fe-UiO-66	Photo-Fenton	[MV] = 20	0.3	160	92	[63]
FeZn-ZIFs	PMS-AOPs	[TC] = 50	0.4	30	92	This study
FeZn-ZIFs	PDS-AOPs	[MV] = 20	0.3	30	94	This study

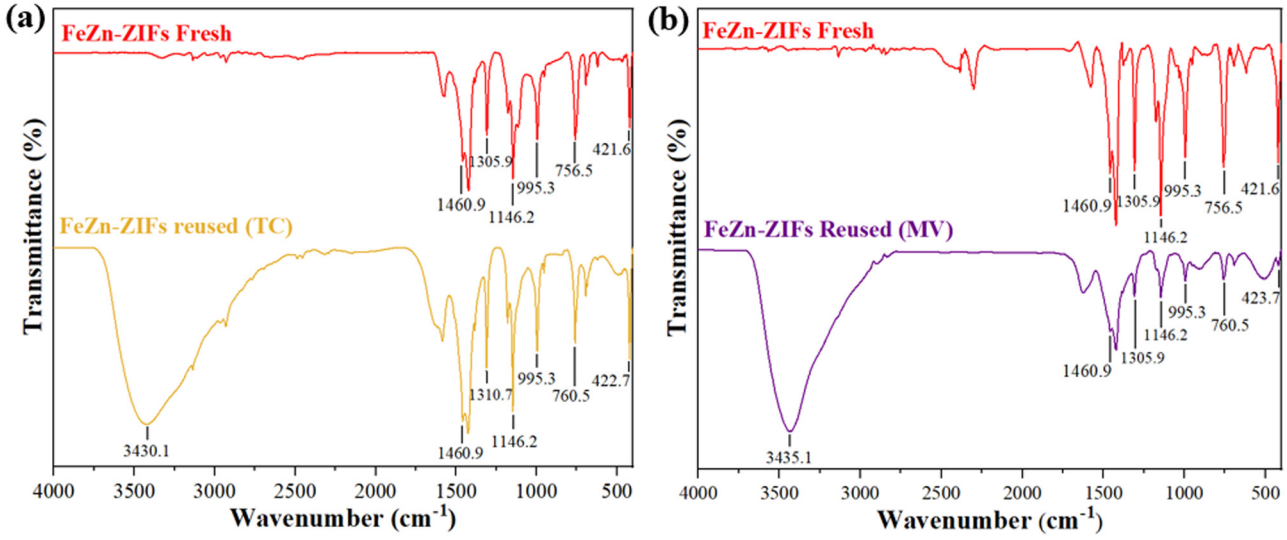

Figure 8: FT-IR spectra of the FeZn-ZIFs reused after removing (a) TC, and (b) MV.

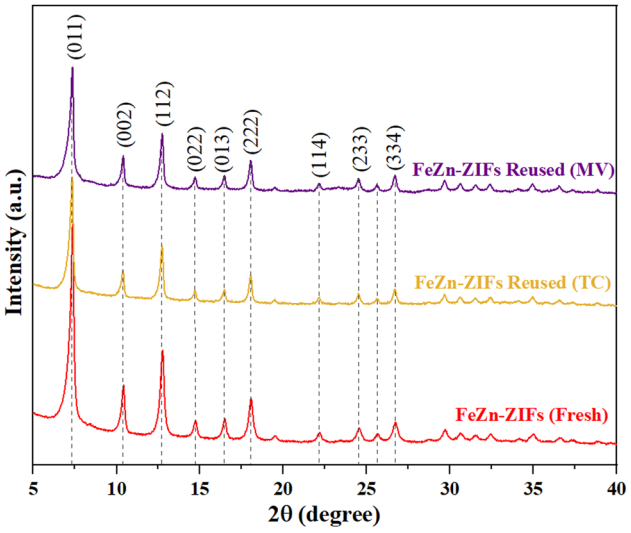

Figure 9: PXRD pattern of FeZn-ZIFs reused after removing TC and MV.

that the structure of FeZn-ZIFs was not destroyed after five times of reusability.

Moreover, the crystallographic structure of the reused FeZn-ZIFs was also examined by PXRD, as shown in Figure 9.

The result revealed the well-defined diffraction peaks implied that the high crystallinity of the samples was maintained. The characteristic peaks were also in good agreement with the original FeZn-ZIFs, but the intensity and width of the peak tended to a slightly different. This can be explained based on the atomic radius of iron before and after performing the catalytic role. Accordingly, the presence of iron in the original bimetallic FeZn-ZIFs had a valence of II, but after the reaction, it was predicted that Fe^{2+} mostly converted to Fe^{3+} [23]. Herein, the Fe^{3+} has an atomic radius of about 0.64 Å, which is much different from that of Fe^{2+} of 1.26 Å, which may create a difference in the crystal structure of FeZn-ZIF compared to the original structure [67].

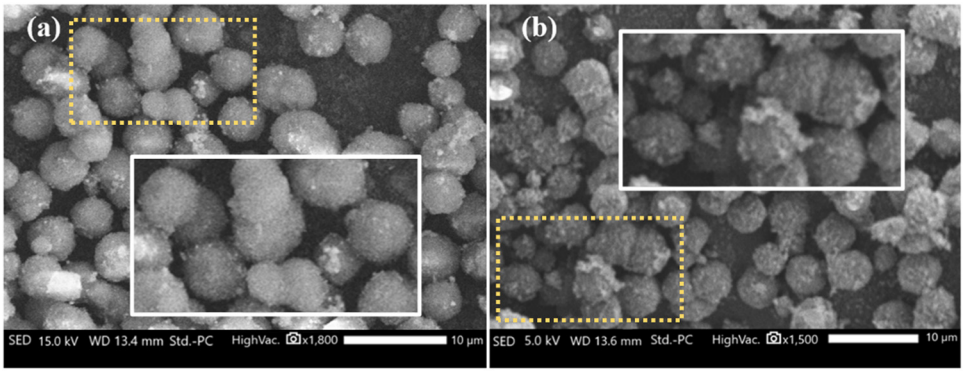

Figure 10: SEM images of the FeZn-ZIFs reused after removing (a) TC, and (b) MV.

Additionally, the surfaces of reused FeZn-ZIFs were observed through the SEM analysis as displayed in Figure 10.

The results illustrated that after the removal reaction of TC and MV, the appearance coarsened more than for the fresh FeZn-ZIFs. This appearance was most likely because the generated strong oxidizing radicals acted on the surface. However, in general, no noticeable difference was found from the comparison of fresh and used FeZn-ZIFs for removing TC and MV, further confirming the good stability and durability of the bimetallic catalyst.

4 Conclusions

The FeZn-ZIFs catalyst was successfully synthesized by a facile solvothermal process and exhibited excellent oxidizing agent activation performance to eliminate TC and MV from aqueous solutions via AOPs. The physical–chemical properties were demonstrated by a series of characterization techniques, i.e., PXRD, SEM, EDX, BET, FT-IR, and TGA. Moreover, after only 30 min at room temperature, the removal efficiency of TC (50 $mg{\cdot}L^{-1}$) reached 92% with the PMS dosage and the catalyst dosage of 0.4 $g{\cdot}L^{-1}$. Simultaneously, the removal efficiency of MV (20 $mg{\cdot}L^{-1}$) reached 95% with the PDS dosage and catalyst dosage of 0.3 $g{\cdot}L^{-1}$. More significantly, the removal efficiency of TC and MV can still be maintained at about 90% after five catalytic cycles, indicating that the catalyst had good recyclability. In summary, this study has provided an additional potential material for catalytic application, which is not only highly effective in removing antibiotics and dyes but also opens up promising directions in the treatment of persistent organic pollutants in water.

Funding information: This research was supported by B2023-TCT-22 project funding from the Ministry of Education and Training, Vietnam. Thu T. A. Le was funded by the Master, Ph.D Scholarship Programme of Vingroup Innovation Foundation (VINIF), code VINIF.2022.ThS.089.

Author contributions: Thu T. A. Le: writing – original draft, writing – review and editing, visualization; Bao H. Dang: methodology, formal analysis; Thanh Q. C. Nguyen: writing – original draft, writing – review and editing, methodology, visualization, and formal analysis; Dam P. Nguyen: resources; and Giao H. Dang: writing – original draft, writing – review and editing, methodology, resources.

Conflict of interest: Authors state no conflict of interest.

Data availability statement: The data sets generated during and/or analyzed during the current study are available from the corresponding author on reasonable request.

References

[1] Tyagi VK, Lo S-L. Sludge: a waste or renewable source for energy and resources recovery. Renew Sustain Energy Rev. 2013;25:708–28. doi: 10.1016/j.rser.2013.05.029.

[2] Saharan VK, Pandit AB, Satish Kumar PS, Anandan S. Hydrodynamic cavitation as an advanced oxidation technique for the degradation of acid red 88 dye. Ind Eng Chem Res. 2012;51:1981–9. doi: 10.1021/ie200249k.

[3] Lapworth D, Baran N, Stuart M, Ward R. Emerging organic contaminants in groundwater: a review of sources, fate and occurrence. Environ Pollut. 2012;163:287–303. doi: 10.1016/j.envpol.2011.12.034.

[4] French GL. The continuing crisis in antibiotic resistance. Int J Antimicrob Agents. 2010;36:S3–7. doi: 10.1016/S0924-8579(10)70003-0.

[5] Phoon BL, Ong CC, Saheed MSM, Show P-L, Chang J-S, Ling TC, et al. Conventional and emerging technologies for removal of antibiotics from wastewater. J Hazard Mater. 2020;400:122961. doi: 10.1016/j.jhazmat.2020.122961.

[6] Mehra S, Singh M, Chadha P. Adverse impact of textile dyes on the aquatic environment as well as on human beings. Toxicol Int. 2021;28:165. doi: 10.18311/ti/2021/v28i2/26798.

[7] Bağda E, Yabaş E, Karakuş N. Feasibility of tetracycline, a common antibiotic, as chelating agent for spectrophotometric determination of UO_2^{2+} after cloud point extraction. J Radioanal Nucl Chem. 2014;299:1813–20. doi: 10.1007/s10967-013-2839-6.

[8] Xiong H, Zou D, Zhou D, Dong S, Wang J, Rittmann BE. Enhancing degradation and mineralization of tetracycline using intimately coupled photocatalysis and biodegradation (ICPB). Chem Eng J. 2017;316:7–14. doi: 10.1016/j.cej.2017.01.083.

[9] Vinitha G, Ramalingam A. Spectral characteristics and nonlinear studies of methyl violet 2B dye in liquid and solid media. Laser Phys. 2008;18:37–42. doi: 10.1134/S1054660X08010076.

[10] Zeyada H, Habashi A, Makhlouf M, Behairy A, Nasher M. Fabrication, electrical transport mechanisms and photovoltaic properties of methyl violet 2B/n-Si hybrid organic/inorganic solar cell. Microelectron Eng. 2016;163:134–9. doi: 10.1016/j.mee.2016.06.019.

[11] Foroutan R, Mohammadi R, Ahmadi A, Bikhabar G, Babaei F, Ramavandi B. Impact of ZnO and Fe_3O_4 magnetic nanoscale on the methyl violet 2B removal efficiency of the activated carbon oak wood. Chemosphere. 2022;286:131632. doi: 10.1016/j.chemosphere.2021.131632.

[12] Gomes AC, Gonçalves IC, de Pinho MN. The role of adsorption on nanofiltration of azo dyes. J Membr Sci. 2005;255:157–65. doi: 10.1016/j.memsci.2005.01.031.

[13] Payan A, Isari AA, Gholizade N. Catalytic decomposition of sulfamethazine antibiotic and pharmaceutical wastewater using Cu-TiO_2@functionalized SWCNT ternary porous nanocomposite: influential factors, mechanism, and pathway studies. Chem Eng J. 2019;361:1121–41. doi: 10.1016/j.cej.2018.12.118.

[14] Oyewo OA, Elemike EE, Onwudiwe DC, Onyango MS. Metal oxide-cellulose nanocomposites for the removal of toxic metals and dyes

from wastewater. Int J Biol Macromol. 2020;164:2477–96. doi: 10.1016/j.ijbiomac.2020.08.074.
[15] Ho Y-C, Chua S-C, Chong F-K. Coagulation-flocculation technology in water and wastewater treatment. In: Handbook of Research on Resource Management for Pollution and Waste Treatment. Hershey, PA: IGI Global; 2020. p. 432–57.
[16] Sahoo TR, Prelot B. Adsorption processes for the removal of contaminants from wastewater: the perspective role of nanomaterials and nanotechnology. In: Nanomaterials for the Detection and Removal of Wastewater Pollutants. Amsterdam, Netherlands: Elsevier; 2020. pp. 161–222.
[17] Liang C, Wei D, Zhang S, Ren Q, Shi J, Liu L. Removal of antibiotic resistance genes from swine wastewater by membrane filtration treatment. Ecotoxicol Environ Saf. 2021;210:111885. doi: 10.1016/j.ecoenv.2020.111885.
[18] Rout PR, Zhang TC, Bhunia P, Surampalli RY. Treatment technologies for emerging contaminants in wastewater treatment plants: A review. Sci Total Environ. 2021;753:141990. doi: 10.1016/j.scitotenv.2020.141990.
[19] Al-Kdasi A, Idris A, Saed K, Guan CT. Treatment of textile wastewater by advanced oxidation processes - a review. Glob Nest Int J. 2004;6:222–30.
[20] Yang Y, Pignatello JJ, Ma J, Mitch WA. Comparison of halide impacts on the efficiency of contaminant degradation by sulfate and hydroxyl radical-based advanced oxidation processes (AOPs. Environ Sci Technol. 2014;48:2344–51. doi: 10.1021/es404118q.
[21] Deng Y, Zhao R. Advanced oxidation processes (AOPs) in wastewater treatment. Curr Pollut Rep. 2015;1:167–76. doi: 10.1007/s40726-015-0015-z.
[22] Wu X, Sun D, Ma H, Ma C, Zhang X, Hao J. Activation of peroxymonosulfate by magnetic $CuFe_2O_4$@ZIF-67 composite catalyst for the study on the degradation of methylene blue. Colloids Surf A: Physicochem Eng Asp. 2022;637:128278. doi: 10.1016/j.colsurfa.2022.128278.
[23] Wang J, Wang S. Activation of persulfate (PS) and peroxymonosulfate (PMS) and application for the degradation of emerging contaminants. Chem Eng J. 2018;334:1502–17. doi: 10.1016/j.cej.2017.11.059.
[24] Wang N, Zheng T, Zhang G, Wang P. A review on Fenton-like processes for organic wastewater treatment. J Environ Chem Eng. 2016;4:762–87. doi: 10.1016/j.jece.2015.12.016.
[25] Pattengale B, Yang S, Ludwig J, Huang Z, Zhang X, Huang J. Exceptionally long-lived charge separated state in zeolitic imidazolate framework: implication for photocatalytic applications. J Am Chem Soc. 2016;138:8072–5. doi: 10.1021/jacs.6b04615.
[26] Wu R, Fan T, Chen J, Li Y. Synthetic factors affecting the scalable production of zeolitic imidazolate frameworks. ACS Sustain Chem Eng. 2019;7:3632–46. doi: 10.1021/acssuschemeng.8b05436.
[27] Park KS, Ni Z, Côté AP, Choi JY, Huang R, Uribe-Romo FJ, et al. Exceptional chemical and thermal stability of zeolitic imidazolate frameworks. Proc Natl Acad Sci. 2006;103:10186–91. doi: 10.1073/pnas.0602439103.
[28] Zhong G, Liu D, Zhang J. The application of ZIF-67 and its derivatives: adsorption, separation, electrochemistry and catalysts. J Mater Chem A. 2018;6:1887–99. doi: 10.1039/C7TA08268A.
[29] Thomas A, Prakash M. The role of binary mixtures of ionic liquids in ZIF-8 for selective gas storage and separation: a perspective from computational approaches. J Phys Chem C. 2020;124:26203–13. doi: 10.1021/acs.jpcc.0c07090.
[30] Li N, Zhou L, Jin X, Owens G, Chen Z. Simultaneous removal of tetracycline and oxytetracycline antibiotics from wastewater using a ZIF-8 metal organic-framework. J Hazard Mater. 2019;366:563–72. doi: 10.1016/j.jhazmat.2018.12.047.
[31] Tran NT, Nguyen MK. The degradation of organic dye contaminants in wastewater and solution from highly visible light responsive ZIF-67 monodisperse photocatalyst. J Solid State Chem. 2021;300:122287. doi: 10.1016/j.jssc.2021.122287.
[32] Abuzalat O, Tantawy H, Basuni M, Alkordi MH, Baraka A. Designing bimetallic zeolitic imidazolate frameworks (ZIFs) for aqueous catalysis: Co/Zn-ZIF-8 as a cyclic-durable catalyst for hydrogen peroxide oxidative decomposition of organic dyes in water. RSC Adv. 2022;12:6025–36. doi: 10.1039/D2RA00218C.
[33] Yang H, Hu S, Zhao H, Luo X, Liu Y, Deng C, et al. High-performance Fe-doped ZIF-8 adsorbent for capturing tetracycline from aqueous solution. J Hazard Mater. 2021;416:126046. doi: 10.1016/j.jhazmat.2021.126046.
[34] Wang Z, Lai C, Qin L, Fu Y, He J, Huang D, et al. ZIF-8-modified $MnFe_2O_4$ with high crystallinity and superior photo-Fenton catalytic activity by Zn-O-Fe structure for TC degradation. Chem Eng J. 2020;392:124851. doi: 10.1016/j.cej.2020.124851.
[35] Dang HG, Ho NTT, Pham VT, Le TAT, Ta KA. Facile synthesis of bimetallic ZnCo-ZIFs and Ag nanoparticles loading on ZnCo-ZIFs (Ag/ZnCo-ZIFs). Can Tho Univ J Sci. 2020;12:47–53. doi: 10.22144/ctu.jen.2020.023.
[36] Nguyen TQ, Tran HB, Nguyen NK, Nguyen NM, Dang GH. Removal efficiency of dibenzofuran using CuZn-zeolitic imidazole frameworks as a catalyst and adsorbent. Green Process Synth. 2023;12:20228112. doi: 10.1515/gps-2022-8112.
[37] Hu Z, Guo Z, Zhang Z, Dou M, Wang F. Bimetal zeolitic imidazolite framework-derived iron-, cobalt-and nitrogen-codoped carbon nanopolyhedra electrocatalyst for efficient oxygen reduction. ACS Appl Mater Interfaces. 2018;10:12651–8. doi: 10.1021/acsami.8b00512.
[38] Thi Thanh M, Vinh Thien T, Thi Thanh Chau V, Dinh Du P, Phi Hung N, Quang Khieu D. Synthesis of iron doped zeolite imidazolate framework-8 and its remazol deep black RGB dye adsorption ability. J Chem. 2017;2017:5045973. doi: 10.1155/2017/5045973.
[39] Qian X, Wang D, Zhang Y, Wu H, Pennycook SJ, Zheng L, et al. Contrasting roles of small metallic elements M (*M* = Cu, Zn, Ni) in enhancing the thermoelectric performance of n-type PbM 0.01 Se. J Mater Chem A. 2020;8:5699–708. doi: 10.1039/D0TA00174K.
[40] Zhou K, Mousavi B, Luo Z, Phatanasri S, Chaemchuen S, Verpoort F. Characterization and properties of Zn/Co zeolitic imidazolate frameworks vs. ZIF-8 and ZIF-67. J Mater Chem A. 2017;5:952–7. doi: 10.1039/C6TA07860E.
[41] Guo X, Xing T, Lou Y, Chen J. Controlling ZIF-67 crystals formation through various cobalt sources in aqueous solution. J Solid State Chem. 2016;235:107–12. doi: 10.1016/j.jssc.2015.12.021.
[42] Ma Y, Chen F, Yang Q, Zhong Y, Shu X, Yao F, et al. Sulfate radical induced degradation of Methyl Violet azo dye with CuFe layered doubled hydroxide as heterogeneous photoactivator of persulfate. J Environ Manag. 2018;227:406–14. doi: 10.1016/j.jenvman.2018.08.030.
[43] Li J, Yang L, Lai B, Liu C, He Y, Yao G, et al. Recent progress on heterogeneous Fe-based materials induced persulfate activation for organics removal. Chem Eng J. 2021;414:128674. doi: 10.1016/j.cej.2021.128674.
[44] Shukla P, Sun H, Wang S, Ang HM, Tadé MO. Co-SBA-15 for heterogeneous oxidation of phenol with sulfate radical for

wastewater treatment. Catal Today. 2011;175:380–5. doi: 10.1016/j.cattod.2011.03.005.
[45] Duan X, Su C, Zhou L, Sun H, Suvorova A, Odedairo T, et al. Surface controlled generation of reactive radicals from persulfate by carbocatalysis on nanodiamonds. Appl Catal B Environ. 2016;194:7–15. doi: 10.1016/j.apcatb.2016.04.043.
[46] Fordham J, Williams HL. The persulfate-iron (II) initiator system for free radical polymerizations1. J Am Chem Soc. 1951;73:4855–9. doi: 10.1021/ja01154a114.
[47] Luo C, Ma J, Jiang J, Liu Y, Song Y, Yang Y, et al. Simulation and comparative study on the oxidation kinetics of atrazine by UV/H_2O_2, UV/HSO_5^- and UV/$S_2O_8^{2-}$. Water Res. 2015;80:99–108. doi: 10.1016/j.watres.2015.05.019.
[48] Xie P, Ma J, Liu W, Zou J, Yue S, Li X, et al. Removal of 2-MIB and geosmin using UV/persulfate: contributions of hydroxyl and sulfate radicals. Water Res. 2015;69:223–33. doi: 10.1016/j.watres.2014.11.029.
[49] Hadjltaief HB, Da Costa P, Beaunier P, Gálvez ME, Zina MB. Fe-clay-plate as a heterogeneous catalyst in photo-Fenton oxidation of phenol as probe molecule for water treatment. Appl Clay Sci. 2014;91:46–54. doi: 10.1016/j.clay.2014.01.020.
[50] Hassan H, Hameed B. Fenton-like oxidation of acid red 1 solutions UsingHeterogeneous catalyst based on ball clay. Int J Environ Sci Dev. 2011;2:218.
[51] Oh W-D, Lim T-T. Design and application of heterogeneous catalysts as peroxydisulfate activator for organics removal: an overview. Chem Eng J. 2019;358:110–33. doi: 10.1016/j.cej.2018.09.203.
[52] Sharma G, Bhogal S, Kumar A, Naushad M, Sharma S, Ahamad T, et al. AgO/MgO/FeO@Si_3N_4 nanocomposite with robust adsorption capacity for tetracycline antibiotic removal from aqueous system. Adv Powder Technol. 2020;31:4310–8. doi: 10.1016/j.apt.2020.09.006.
[53] Zhou Y, Feng S, Duan X, Wu W, Ye Z, Dai X, et al. Stable self-assembly Cu_2O/ZIF-8 heterojunction as efficient visible light responsive photocatalyst for tetracycline degradation and mechanism insight. J Solid State Chem. 2022;305:122628. doi: 10.1016/j.jssc.2021.122628.
[54] Ma W, Zhu Y, Wang X. Au nanoparticles modified HNTs/g-C_3N_4/CdS composite for highly efficient CO_2 photoreduction and tetracycline degradation. J Alloy Compd. 2023;935:168129. doi: 10.1016/j.jallcom.2022.168129.
[55] Hu T, Deng F, Feng H, Zhang J, Shao B, Feng C, et al. Fe/Co bimetallic nanoparticles embedded in MOF-derived nitrogen-doped porous carbon rods as efficient heterogeneous electro-Fenton catalysts for degradation of organic pollutants. Appl Mater Today. 2021;24:101161. doi: 10.1016/j.apmt.2021.101161.
[56] Wang M, Wang Y, Li Y, Wang C, Kuang S, Ren P, et al. Persulfate oxidation of tetracycline, antibiotic resistant bacteria, and resistance genes activated by Fe doped biochar catalysts: Synergy of radical and non-radical processes. Chem Eng J. 2023;464:142558. doi: 10.1016/j.cej.2023.142558.
[57] Xu D, Yang T, Dong Y, Wang Q, Zhu J, Zhang G, et al. Activation of peroxymonosulfate by CoP@ Co_2P heterostructures via radical and non-radical pathways for antibiotics degradation. Ceram Int. 2023;49:16999–7007. doi: 10.1016/j.ceramint.2023.02.062.
[58] Shamsipur M, Rajabi HR. Study of photocatalytic activity of ZnS quantum dots as efficient nanoparticles for removal of methyl violet: effect of ferric ion doping. Spectrochim Acta Part A: Mol Biomol Spectrosc. 2014;122:260–7. doi: 10.1016/j.saa.2013.11.064.
[59] Liu Y, Ding S, Xu J, Zhang H, Yang S, Duan X, et al. Preparation of a pn heterojunction $BiFeO_3$@TiO_2 photocatalyst with a core–shell structure for visible-light photocatalytic degradation. Chin J Catal. 2017;38:1052–62. doi: 10.1016/S1872-2067(17)62845-6.
[60] Saeed K, Khan I, Gul T, Sadiq M. Efficient photodegradation of methyl violet dye using TiO_2/Pt and TiO_2/Pd photocatalysts. Appl Water Sci. 2017;7:3841–8. doi: 10.1007/s13201-017-0535-3.
[61] Saravan RS, Muthukumaran M, Mubashera S, Abinaya M, Prasath PV, Parthiban R, et al. Evaluation of the photocatalytic efficiency of cobalt oxide nanoparticles towards the degradation of crystal violet and methylene violet dyes. Optik. 2020;207:164428. doi: 10.1016/j.ijleo.2020.164428.
[62] Kaci M, Nasrallah N, Djaballah A, Akkari I, Belabed C, Soukeur A, et al. Insights into the optical and electrochemical features of $CuAl_2O_4$ nanoparticles and it use for methyl violet oxidation under sunlight exposure. Opt Mater. 2022;126:112198. doi: 10.1016/j.optmat.2022.112198.
[63] Hosseini M-S, Abbasi A, Masteri-Farahani M. Improving the photocatalytic activity of NH_2-UiO-66 by facile modification with Fe(acac)$_3$ complex for photocatalytic water remediation under visible light illumination. J Hazard Mater. 2022;425:127975. doi: 10.1016/j.jhazmat.2021.127975.
[64] Karakas K, Celebioglu A, Celebi M, Uyar T, Zahmakiran M. Nickel nanoparticles decorated on electrospun polycaprolactone/chitosan nanofibers as flexible, highly active and reusable nanocatalyst in the reduction of nitrophenols under mild conditions. Appl Catal B: Environ. 2017;203:549–62. doi: 10.1016/j.apcatb.2016.10.020.
[65] Abdi J, Mahmoodi NM, Vossoughi M, Alemzadeh I. Synthesis of magnetic metal-organic framework nanocomposite (ZIF-8@SiO_2@$MnFe_2O_4$) as a novel adsorbent for selective dye removal from multicomponent systems. Microporous Mesoporous Mater. 2019;273:177–88. doi: 10.1016/j.micromeso.2018.06.040.
[66] Mohammed YA, Abdel-Mohsen A, Zhang Q-J, Younas M, Zhong L-B, Yang J-CE, et al. Facile synthesis of ZIF-8 incorporated electrospun PAN/PEI nanofibrous composite membrane for efficient Cr(VI) adsorption from water. Chem Eng J. 2023;461:141972. doi: 10.1016/j.cej.2023.141972.
[67] Sun X, Xu C, Tian G, Rao L. Complexation of glutarimidedioxime with Fe(III), Cu(II), Pb(II), and Ni(II), the competing ions for the sequestration of U (VI) from seawater. Dalton Trans. 2013;42:14621–7. doi: 10.1039/C3DT51767E.